Journal of the Korean Nuclear Society
Volume 32, Number 6, pp.618~635, December, 2000

KAIST-CIWH Computer Code and a Guide Chart to Avoid Condensation-Induced Water Hammer in Horizontal Pipes

Moon-Hyun CHUN and Seon-Oh YU
Korea Advanced Institute of Science and Technology
373-1, Kusong-Dong, Yusong-Gu, Taejon, 305-701, Korea
chunmh@kaist.ac.kr

(Received June 22, 2000)

Abstract

A total of 17 experimental data for the onset of slugging, which is assumed to be the precursor of the condensation-induced waterhammer (CIWH), have been obtained for various flow rates of water. Incorporating the most recent correlations of interfacial heat transfer and friction factor developed for a circular geometry and using an improved criterion of transition from stratified to a slug flow, two existing analytical models to predict lower and upper bounds for CIWH have been upgraded. Applicability of the present as well as existing CIWH models has been tested by comparison with two sets of CIWH data. The result of this comparison shows that the applicability of the present as well as existing models is reasonably good. Based on the present models for CIWH, a computer code entitled as "KAIST-CIWH" has been developed and sample guide charts to find CIWH free regions for a given combination of major flow parameters in a long horizontal pipe have been presented along with the results of parametric studies of major parameters (D, P, $T_{f,in}$, and L/D) on the critical inlet water flow rate$(W_{f,in})_{crit}$ for both lower and upper bounds. In addition, two simple formulas for lower and upper bounds that can be used in an emergency for quick results have been presented.

Key Words : Condensation-induced water hammer (CIWH), Lower and upper bounds for CIWH, Onset of slug flow, Steam-water stratified countercurrent two-phase flow

1. Introduction

In the past three decades, since a large number of water hammer events occurred in the light-water-reactor (LWR) power plants, a number of comprehensive studies on the phenomena assocciated with water hammer events have been performed. The mechanisms for initiating water hammer in nuclear power plants have been classified into nine different categories by recent studies. However, Yow et al. [1] noted that there are three basic types of severe water hammer occurring at power plants that can result in significant plant damage: rapid valve operation events, water-slug-induced events, and condensation-induced events. They also found that

Table 1. Test Matrix for Present Experiments

	Test Section				j_f [m/s]	Re_f	j_g [m/s]	No.of Data
	D [m]	L [m]	L/D	Inclination Angle				
Steam/ Water Test	0.0830.	2.2	26.5	0.5°	0.02 ~0.10	1628.3 ~12473.5	0~7.67 (up to the onset of slugging)	17

condensation-induced water hammers (CIWHs) were responsible for about 34 percent of the 283 events compiled by Van Duyne et al. [2]. The mechanisms associated with these CIWHs include the following [1]: ① steam and water counter-flow in a horizontal pipe, ② subcooled water with condensing steam in a vertical pipe (water cannon), ③ pressurized water entering a vertical, steam-filled pipe, and ④ hot water entering a lower pressure line. A significant event which occurred at San Onofre Unit 1, in particular, is an example of the first mechanism. Owing to many exhaustive studies on this subject [3,4,5], now it is well understood that the condensation process for the steam and subcooled water counterflow in a horizontal pipe will result in two-phase flow interfacial instability, and is capable of initiating a severe water hammer that will result in significant plant damage.

Although a number of earlier studies identified basic mechanisms for various types of water hammer initiation and presented some important strategies for avoiding water hammer initiating events [2-4], no analytical model for the CIWH in a long horizontal or nearly horizontal pipe can be found at this time except the one presented by Bjorge and Griffith [5]. The analytical method used by Bjorge and Griffith [5] follows that of Linehan et al. [6]. Their model used one-dimensional flow equations and empirical correlations of interfacial shear stress and heat and mass transfer available at that time. The criterion of transition from stratified to slug flow was calculated by the Taitel-Dukler criterion [7] with local steam flow rates and liquid depth obtained from the flow equations. The results of calculation compared favorably to the experimental data. The effects of varying the inlet water subcooling, the pipe length, and the pipe diameter on the initiation of water slug were also studied with the verified analytical model.

The purpose of this work is to upgrade the existing analytical models to obtain the critical inlet water flow rates $(W_{f,in})_{crit}$ of CIWH for both lower and upper bounds in a long horizontal pipe by incorporating empirical correlations of interfacial friction factor (f_i) and heat transfer (h_i) developed most recently for a circular pipe geometry and using an improved criterion of transition from stratified to a slug flow. A series of experiments were performed to obtain experimental data for the onset of slugging and predictions of representative models are compared against present experimental data. Applicability of the CIWH models has been tested by comparison with CIWH data. Based on the present models, a computer code entitled as "KAIST-CIWH" has been developed and sample guide charts to avoid the CIWH for a given combination of flow parameters in a long horizontal circular pipe are presented. In addition, two simple formulas for lower and upper bounds of the CIWH to be used for quick results in an emergency are also presented.

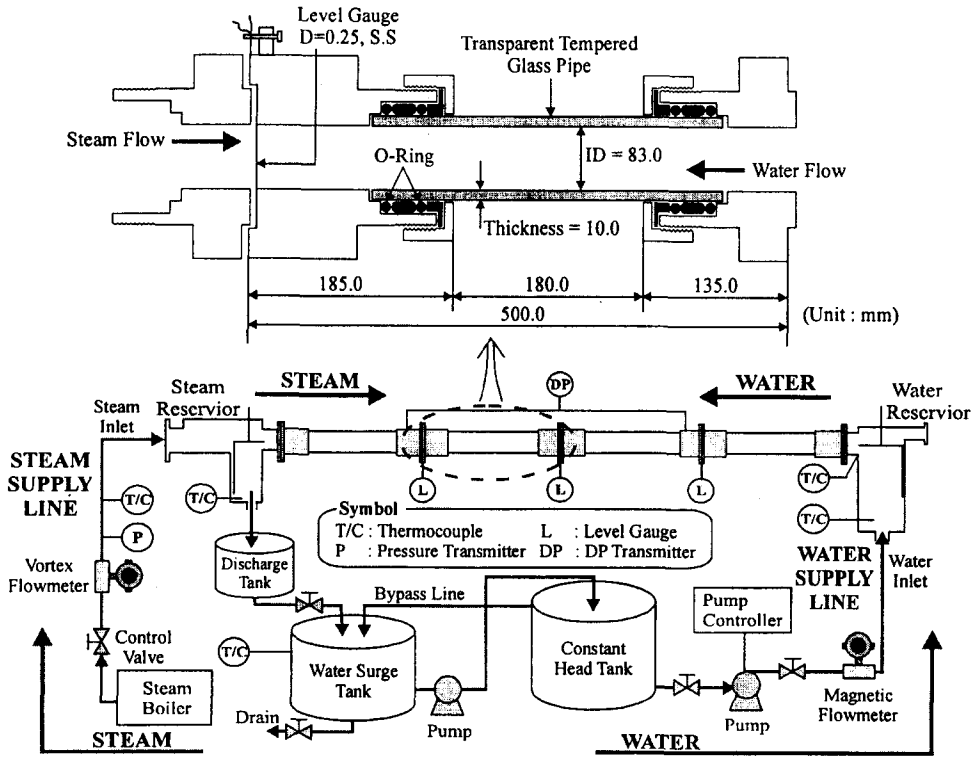

Fig. 1. Schematic Diagram of Experimental Apparatus

2. Experiments

A series of experiments were performed and a total of 17 experimental data for the onset of slugging, which is assumed to be the precursor of the CIWH in the present work, in nearly horizontal countercurrent two-phase flow have been obtained for various flow rates of water. The test matrix is shown in Table 1.

2.1. Experimental Apparatus

A schematic diagram of the experimental apparatus is shown in Fig. 1. The main components were ① the test section, ② the steam and the water supply systems, ③ sensors and devices to measure the water level and flow rates, and ④ the data acquisition system.

The test section is slightly inclined (0.5° from the water inlet) and consists of four transparent tempered glass pipes which are connected in series by flanges. The total length and inner diameter of the horizontal channel are 2.2 *m* and 0.083 *m*, respectively. While the saturated steam was supplied by a 200 *kW* electric steam boiler, filtered tap water was pumped from the water surge tank to the test section. The flow rates of steam and water were measured by a vortex and a magnetic flowmeters, respectively: The accuracy of the vortex and the magnetic flowmeters were within $\pm 1.0\%$ and $\pm 0.5\%$, respectively. The inlet temperatures of steam and water were also measured by *k*-type thermocouples installed at the downstream of the vortex flowmeter and inside

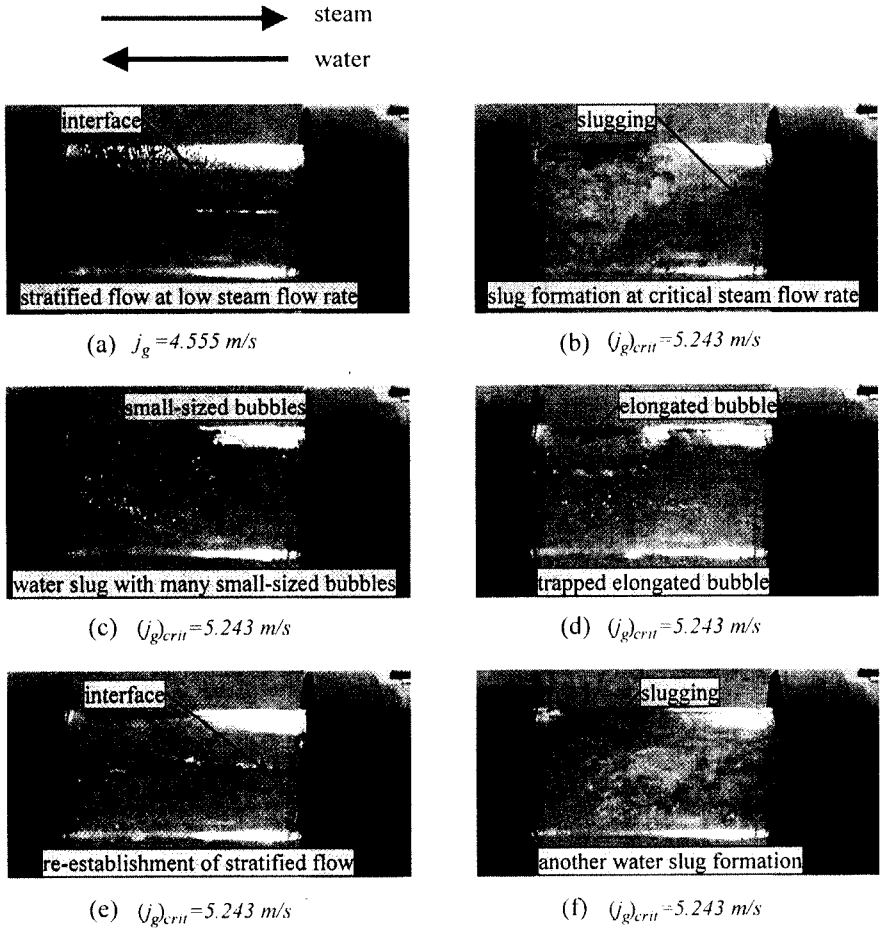

Fig. 2. Photographs Showing the Sequence of Slug Formation in a Pipe (j_f =0.091 m/s)

the water reservoir, respectively. The instantaneous water level was evaluated by measuring the electrical resistance which varies according to the changes in the water level difference between two vertical parallel electrodes inserted in the test section. The electrodes consisted of two stainless steel wires of 0.25 *mm* in diameter, mounted vertically in the test section about 5 *mm* apart in a plane perpendicular to the direction of the flow. Because of the variation of the conductivity with temperature and impurities, the level sensors were calibrated for each run and also checked repeatedly during the test : The response of this level gauge was quite linear and the average standard deviation was about 0.5 *mm*.

2.2. Test Parameters and Test Procedure

The major test parameters in the present experiment were the inlet flow rates of steam and water, and the water level. A total of 17 runs were made under atmospheric pressure condition as summarized in Table 1. The range of superficial velocity of water (j_f) was 0.02 ~ 0.10 *m/s*, whereas that of steam (j_g) was 0.00 ~ 7.67 *m/s*.

The experimental procedure for a given test is

as follows: ① The inlet water flow rate was first set to a specified value. ② The steam flow rate was then increased in small steps until the onset of slugging occurred. ③ After allowing a sufficient time to reach a quasi-steady state, the time averaged water level and flow rates were taken. The same procedure has been repeated for all the tests.

The onset of slugging was readily determined by direct visual observation as a slight increase in steam flow rate at the onset of slugging resulted in a dramatic change in the flow pattern. In addition, the reproducibility of the present experimental data has been confirmed by repeating the same test three times under typical test conditions: The ranges of standard deviation of j_f and $(j_g)_{crit}$ evaluated for two sets of reproducibility tests were 0.0007 ~ 0.002 and 0.18 ~ 0.20, respectively.

2.3. Observation of Slug Formation and water hammer initiation

Photographs of steam-water interactions in the test section were taken for two different conditions, one for a low steam flow rate (j_g =4.555 *m/s*) and the other for a critical steam flow rate (j_g =4.243 *m/s*) where a CIWH occurred. Figure 2(a) shows the case of low steam flow rate: The steam-water interface is clearly visible and small ripples appear at the steam inlet and slowly propagates toward the water inlet. A typical case of critical steam flow rate, on the other hand, is shown in Figs. 2(b) (2(f). These five photographs show the process of CIWH formation:

① At the critical steam flow rate, when the wave grows large enough to fill the pipe cross section, eventually a water slug is formed as can be seen in Fig. 2(b).

② Fig. 2(c) shows that a large number of small steam bubbles are entrained in the water slug and the water slug carries the water toward the steam flow direction.

③ As can be seen in Fig. 2(d), the water slug traps a large steam bubble (elongated bubble), which condenses and collapses rapidly causing a condensation-induced water hammer.

④ Then gravity waves originate from this discontinuity, seeking to re-establish a stratified flow and this process is shown in Fig. 2(e).

⑤ Another water slug is formed before the large wave (moving toward right) reaches the end of the pipe, and this periodic water hammer continues. Figure 2(f) shows the beginning of another CIWH.

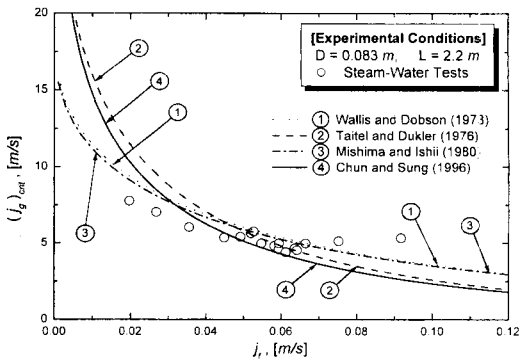

Fig. 3. Dimensional j_f Versus j_g Curves of the Present Onset of Slugging Data and Existing Model Predictions

The present experimental data are shown in the form of dimensional j_g versus j_f curves along with the predictions of representative existing models proposed for the onset of slug flow in Fig. 3. As can be seen in Fig. 3, all the models successfully predict the present data for the onset of slugging or the initiation of CIWH. The agreement between the existing models and data is about the same except that Taitel and Dukler's [7] and Chun and Sung's [8] models slightly underpredict the $(j_g)_{crit}$ values when j_f values are larger than 0.06 *m/s*.

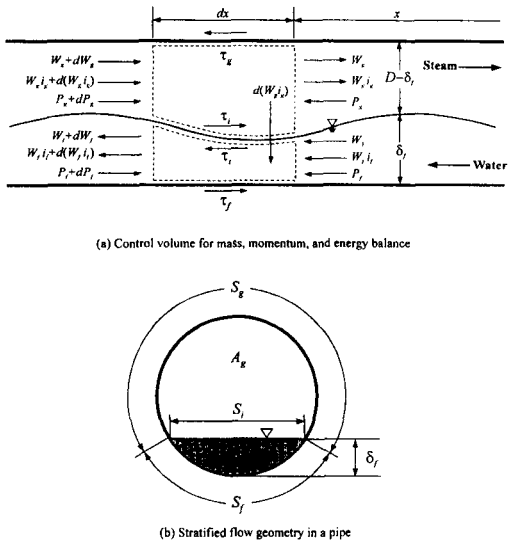

(a) Control volume for mass, momentum, and energy balance

(b) Stratified flow geometry in a pipe

Fig. 4. Model Used for Analysis of Steam-water Countercurrent Flow Induced Water Hammer

3. Analytical Models for Lower and Upper Bounds

The physical phenomena of CIWH in a horizontal pipe can be described by reference to the flow geometry shown in Fig. 4. The steam flow interfering with inlet water flow can form a water slug in the pipe and thereby trap a steam bubble upstream of the water slug. Rapid condensation of the trapped steam bubble by continuous inflow of the subcooled water causes acceleration of the water slug, giving rise to a condensation-induced water hammer. This phenomenon corresponds to a lower bound condition for the initiation of a CIWH.

Inferring from the basic physical phenomena of water hammer and experimental observations, an analytical model to estimate the critical inlet water flow rates for given flow conditions, i.e., a lower limit of the CIWH initiation, is first outlined here.

3.1. Lower Bound

The analytical method to derive the lower bound (where a CIWH is predicted to occur in a long horizontal pipe) follows those of Bjorge and Griffith [5] and Linehan et al. [6] except the following:

① In the expression of the steam condensation rate (see Eq. (A5)), the effect of heat transfer from the steam to the pipe wall is included, whereas this effect was neglected in the earlier works of others [5-6].

② In an effort to upgrade the analytical model and to incorporate current advances made in the understanding of interfacial transport phenomena, correlations of interfacial friction factor (j_i included implicitly in Eq. (A3)) and interfacial heat transfer coefficient (h_i in Eq. (A5)) developed most recently for a steam-water countercurrent flow in circular geometry by present authors [9-10] are used.

③ Also, the criterion for the lower bound of CIWH initiation is based on the stratified-slug flow transition criterion developed most recently by present authors [8].

3.1.1. Governing Equations and Boundary Conditions

The dimensionless governing equations for lower bound are as follows [11]:

$$\left[1-Fr^2(1+\phi)\right]\frac{d\delta_f^*}{dx^*}=2Fr^2q^*(\psi-1)-\tau_i^*-\tau_f^*-\tau_g^*-\dot{\theta} \quad (1)$$

$$\frac{dT_f^*}{dx^*}=q^*\left(\frac{DS_i}{A_f}\right)\left(\frac{\beta_1}{\beta_0}\right) \quad (2)$$

$$W_g^*=\frac{W_{g,in}}{W_{f,in}}+\frac{\beta_2}{\beta_1} \quad (3)$$

The applicable boundary conditions are:

$$T_f^* = 0,\ W_g^* = 0 \quad \text{at } x^* = 0 \tag{4}$$

$$1 - Fr^2(1+\phi) = 0 \quad \text{at } x^* = \frac{L}{D} \tag{5}$$

The definitions of these dimensionless variables are summarized in Appendix A. In the above dimensionless governing equations (Eq. (1)~((3)), there are three dependent variables, δ_f^*, T_f^* and W_g^*. Before these equations can be solved simultaneously to obtain the three unknowns, the quantities of τ_f, τ_i, and τ_g in Eq. (A3) and h_i and h_{wa} in Eq.(A5) must be specified using appropriate correlations. The constitutive relations used in the derivations of lower and upper bounds are given in Appendix B.

3.1.2. Criterion for the Condensation-induced Water Hammer Initiation

In a manner similar to the methods used by earlier workers [5,11], a localized water slug formation is assumed to lead to a CIWH in a long horizontal pipe. To obtain the lower bound for CIWH initiation, the criterion of stratified-slug flow transition for a horizontal or a nearly horizontal pipe proposed by Chun and Sung [8], is first transformed into the following form:

$$N_{CIWH} = \frac{\phi Fr^2}{(1-\delta_f^*)^2 \cos\theta\, C} \geq 1.0 \tag{6}$$

where

$$C = 1 + \frac{1-\alpha}{\alpha}\frac{\rho_g}{\rho_f} \tag{7}$$

When $N_{CIWH} \geq 1.0$ at any location along the pipe, a localized water slug formation is assumed to lead to a CIWH.

3.2. Upper Bound

When the injected water flow rate is large enough, the reduction rate in the steam volume due to refilling is approximately equal to the amount of condensation on the steam-water interface and the pipe wall. At this point, the net steam flow into the pipe is approximately zero and is not large enough to generate a water slug. In other words, if the inlet water flow rate exceeds the condensation rate (i.e., $W_{f,in} \geq W_c$), then no net steam will flow into the pipe, and water hammer will not occur. Thus, an upper bound may be obtained from the following relations:

The mass of steam is balanced by the condensation rate.

$$-\frac{d(\rho_g V_g)}{dt} = W_c = \frac{h_i S_i L (T_g - T_f) + h_{wa} S_g L (T_g - T_{wa})}{i_{fg}} \tag{8}$$

Eq. (8) assumes that the steam is condensed on both the water surface and the pipe wall. Then, an approximate expression for the upper bound criterion to avoid water hammer is

$$W_{f,in} \geq W_c \tag{9}$$

The water depth, in addition, can be obtained from the solution of the following equations:

$$\frac{Fr^2 g A_f^3 \rho_f^2}{2W_f^2} - D\sqrt{\delta_f^* - \delta_f^{*2}} = 0 \tag{10}$$

where W_f can be determined by

$$\frac{W_f}{W_{f,in}} = \frac{i_{fg} + C_{Pf}(T_g - T_{f,in})}{i_{fg} + C_{Pf}(T_g - T_f)} \tag{11}$$

Eq. (10) is derived from the Froude number defined by Eq. (A8) in Appendix A, whereas Eq. (11) is obtained from the mass and the energy balance equations for the control volume of both phases.

3.3. Numerical procedures

To obtain the lower bound for a given condition, the governing equations with the given boundary conditions should be solved numerically. In the present study, after the nodalization of the given pipe, the finite difference method (FDM) was used and the values of the major dependent variables δ_f^*, T_f^*, and W_g^* were calculated at every node. The 8 steps of overall calculation procedure is as follows:

Step 1: Leftward Sweep (increasing direction of x^*):

Using the FDM, Eq. (2) is expressed as follows:

$$(T_f^*)_{n+1} = (T_f^*)_n + \left[q^* \left(\frac{DS_i}{A_f} \right) \left(\frac{\beta_1}{\beta_0} \right) \right]_n \left[(x^*)_{n+1} - (x^*)_n \right] \quad (12)$$

where n is the node identification. To solve Eq. (12), Eqs. (3) and (4) are used along with the starting value of $(\delta_f^*)_n = 0.5$

Step 2: Flow parameters and properties included in the governing equations, i.e., those values defined by Eqs. (A3) ~ (A6), and (A8), are calculated for node $(n+1)$ with $(T_f^*)_{n+1}$.

Step 3: The water level of the last node, $(\delta_f^*)_{n=N}$ that satisfies Eq. (5) is then obtained by Newton-Raphson method.

Step 4 : Rightward Sweep (decreasing direction of x^*):

Eq. (1) is first expressed in finite difference form as follows:

$$(\delta_f^*)_{n-1} = (\delta_f^*)_n - \left[\frac{2Fr^2 q^* (\psi - 1) - \tau_i^* - \tau_f^* - \tau_g^* - \theta}{1 - Fr^2 (1 + \phi)} \right]_n \left[(x^*)_n - (x^*)_{n-1} \right] \quad (13)$$

The $(\delta_f^*)_{n=N}$ value for the last node obtained in Step 3, along with other flow parameters and properties, is then substituted into Eq. (13) to obtain the dimensionless water depth at $(n-1)$ node, $(\delta_f^*)_{n-1}$.

Step 5: Flow parameters and properties included in the governing equations are evaluated again for node $(n-1)$ using $(\delta_f^*)_{n-1}$.

Step 6: The above calculation procedure is repeated until the following two conditions of convergence are satisfied at j the calculation.

$$\frac{(T_f^*)_n^j - (T_f^*)_n^{j-1}}{(T_f^*)_n^j} \le \varepsilon, \quad n = 1,2,\cdots,N \quad (14)$$

$$\frac{(\delta_f^*)_n^j - (\delta_f^*)_n^{j-1}}{(\delta_f^*)_n^j} \le \varepsilon, \quad n = 1,2,\cdots,N \quad (15)$$

Step 7: When a set of solutions for the dependent variables (δ_f^*, T_f^* and W_g^*) are obtained, the stability parameter N_{CIWH} given by Eq. (6) is calculated for each node.

Step 8: By varying the inlet water flow rate, the above procedure is repeated until the calculated maximum N_{CIWH} value just exceeds unity at any node. The localized water slug formation, which is assumed to be leading to a CIWH, is then predicted when there is any $N_{CIWH} \ge 1.0$ value at any node.

The water depth and the critical inlet water flow rate that satisfy the upper bound of CIWH given by Eq. (9) can be obtained in a manner similar to the numerical procedure used for the lower bound. That is, Eq. (10) can be solved by the Newton-Raphson method to find the critical inlet water flow rate for the upper bound.

4. Results and Discussions

4.1. Assessment of Present Model

Present and representative existing analytical models for CIWH initiation have been examined for their applicability using an actual water

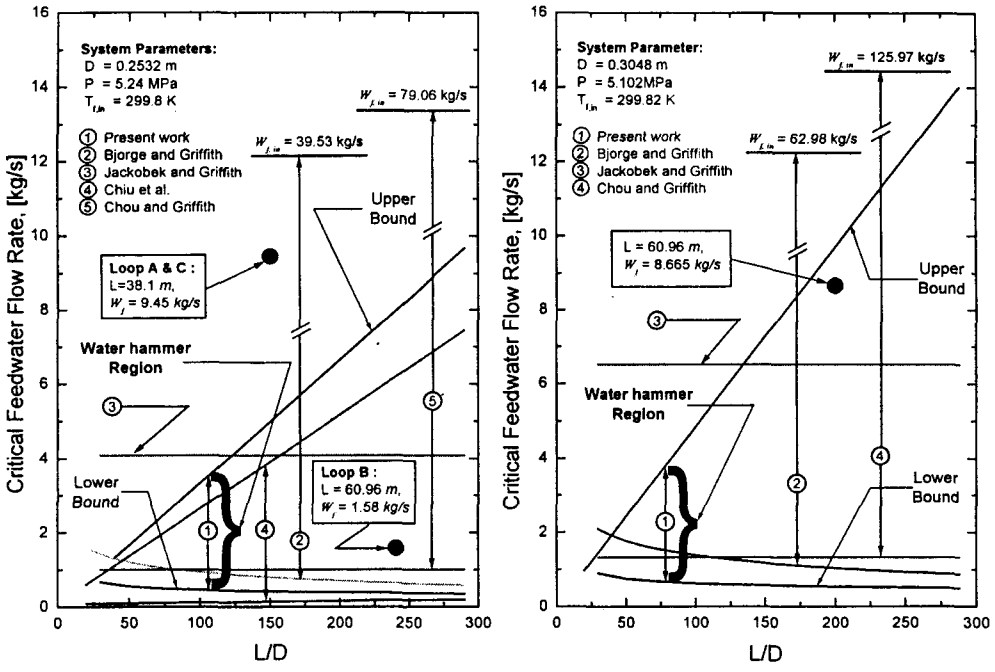

(a) SONG-1 event (b) Izenson et al.'s sample case study

Fig.5 Comparison of Water Hammer Region Boundaries Predicted by Various Analytical Models for Two Events: (a) SONG-1 Event, and (b) Izenson et. al.'s sample case study

hammer event of SONG-1 [12] and the sample case study of Izenson et al. [4]. Figures 5(a) and 5(b) show critical inlet feedwater flow rates, $(W_{f,in})_{crit}$, as a function of the pipe length to diameter ratio (L/D) along with water hammer region boundaries predicted by various models for two CIWH events.

For the actual water hammer event of SONG-1, loops A and C (each about 38.10 *m* in length) were about half the length of loop B (~60.96 *m*), and the two loops A and C were completely filled at a high auxiliary feedwater flow rate (9.45 *kg/s*) while the loop B was filling at a low auxiliary feedwater flow rate (1.58 *kg/s*) at the time of the water hammer. The reason why a severe water hammer occurred only in the main feedwater line B, even though all three feedwater lines (A, B, and C) of the SONG-1 were partially or completely voided and then refilled during the event, can be explained as follows: For the flow rate larger than the upper bound, the net steam flow will reverse its direction and move toward the steam generator, and the water slug generated will tend to move out of the horizontal feedwater line and flow toward the steam generator. In this case, because of the presence of large amount of steam, it will be impossible to form a low-pressure zone in front of the water slug, and therefore, the water slug will not be accelerated and collapse. Figure 5(a) shows that loops A and C were operated well outside the region bounded by lower and upper critical inlet feedwater flow rates. The condition of the loop B, however, falls within the lower and upper bounds where water hammer can occur. Figure 5(a) also shows that the lower bound obtained from the present model is slightly lower

Table 2. Ranges of Parameters Examined

System Parameters	Range	No. of Cases
Pipe diameter [m]	0.10 ~ 0.75	12
System pressure [MPa]	0.1 ~ 16	5
Inlet feedwater temperature [°C]	10 ~ 50	5
Ratio of length to diameter (L/D)	30 ~ 250	12
Total number of cases (Lower + Upper)		7200 (=3600 x 2)

than that from Bjorge and Griffith's 'absolute stability limit' [5], whereas the upper bound predicted by present model is slightly higher than that by Chiu et al. [12]. Bjorge and Griffith [5] and Chou and Griffith [13] used the pipe run full criterion with Froude number of 0.5 and 1.0, respectively, in their prediction of the upper bound, and both results overpredicted the upper limit of the water hammer region. Chou and Griffith [13] and Jackobek and Griffith [14] did not consider the pipe length in their analysis. Also, the lower bound model of Chiu et al. [12] shows that increasing the *L/D* slightly increases the critical inlet water flow rate for water hammer initiation as opposed to the predictions of the present as well as Bjorge and Griffith [5] models as can be seen Fig. 5(a).

The result of another CIWH analyses performed for the sample case study of Izenson et al. [4], whose scenario is similar to the SONG-1 event except for its detailed conditions, is shown in Fig. 5(b): The effective length of the feedwater line, from the isolation valve to the riser at the steam generator, is about 60.96 *m* and the diameter is 0.3048 *m*. The void fraction in the pipe at the time of the water hammer is 0.17, which means that the pipe is almost full. As shown in Fig. 5(b), the data point falls within the region bounded by lower and upper bounds, and the predicted location on the critical feedwater flow rate versus *L/D* curve is closer to the upper boundary limit. In general, the lower and upper bounds obtained by various models are similar to the case of the actual water hammer event of SONG-1.

4.2. Parametric Effects on CIWH

The effects of major system parameters, i.e., ① the pipe diameter (*D*), ② the pipe length to pipe diameter ratio (*L/D*), ③ the system pressure (*P*), and ④ the inlet feedwater temperature ($T_{f,in}$), on the critical inlet feedwater flow rate ($(W_{f,in})_{crit}$) are shown in Figs. 6~8. The ranges of parameters considered in the lower and upper bounds analysis, on the other hand, are summarized in Table 2. From the results of present analysis shown in Figs. 6~8, major parametric effects can be summarized as follows:

① For a given *L/D*, as the pipe diameter (*D*) is increased, the critical feedwater flow rate, $(W_{f,in})_{crit}$, increases for both lower and upper bounds as can be observed in Figs. 6(a,b).

② However, Figs. 6(a,b), 7(a,b), and 8(a,b) show that for a given pipe diameter or system pressure and/or inlet feedwater temperature, $(W_{f,in})_{crit}$ for upper bound increases linearly, while $(W_{f,in})_{crit}$ for lower bound decreases, when *L/D* is increased.

③ Figures 7(a,b) show that increasing the system pressure (*P*), $(W_{f,in})_{crit}$ for upper bound increases, while that for lower bound decreases.

④ Figures 8(a,b), on the other hand, show that

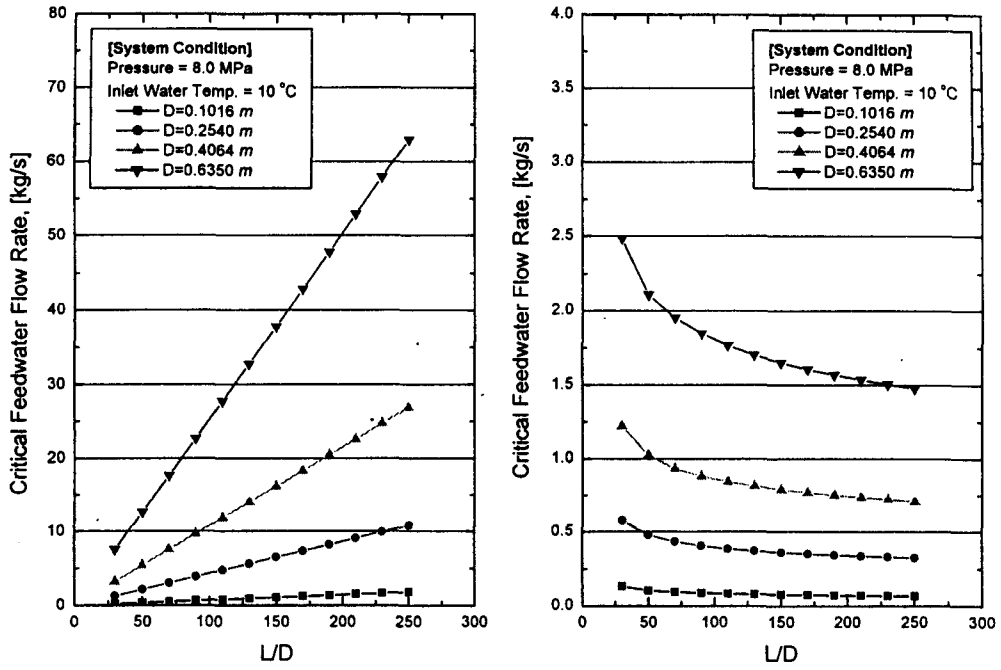

(a) Upper bound (b) Lower bound

Fig. 6 Effect of Pipe Diameter on $(W_{f,in})_{crit}$ for Lower and Upper Bounds

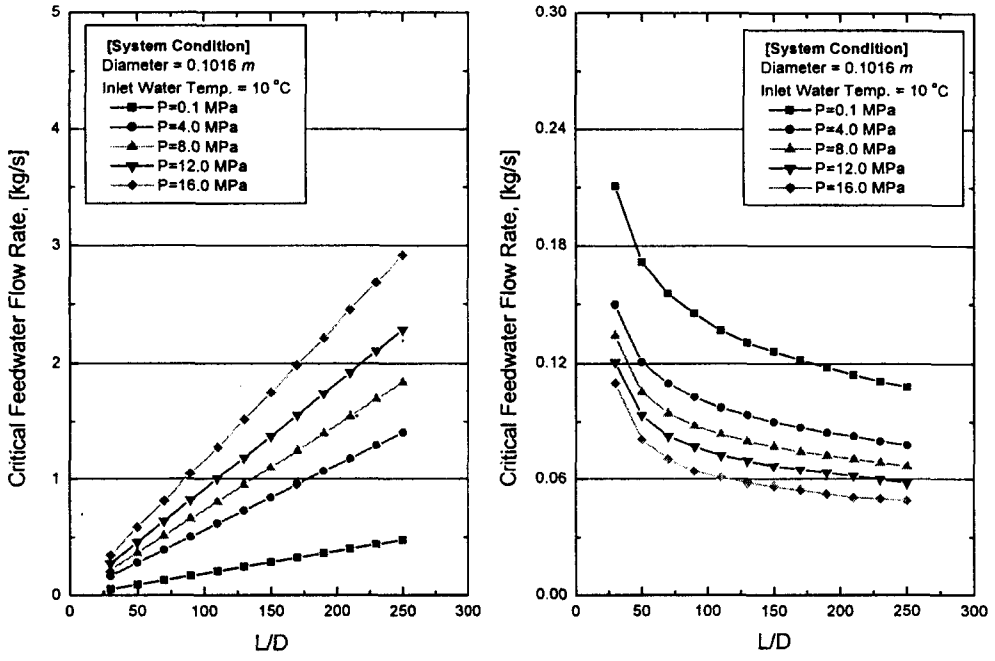

(a) Upper bound (b) Lower bound

Fig. 7 Effect of System Pressure on $(W_{f,in})_{crit}$ for Lower and Upper Bounds

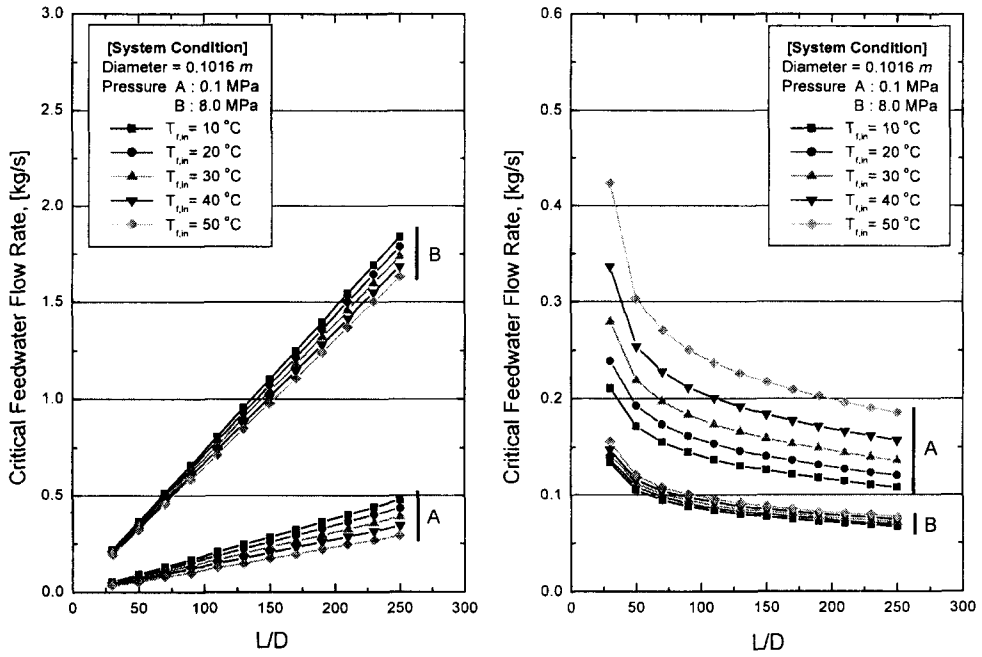

(a) Upper bounds (b) Lower bounds

Fig. 8 Effect of Inlet Feedwater Temperature $(W_{f,in})_{crit}$ on for Lower and Upper Bounds

decreasing the feedwater inlet temperature, $(W_{f,in})_{crit}$ for upper bound increases, whereas that for lower bound decreases. Figures 8(a,b) also show that the effect of the inlet feedwater temperature on $(W_{f,in})_{crit}$ is relatively smaller at higher system pressure (e.g., 8.0 MPa) than at lower pressure (e.g., 0.1 MPa).

4.3. A guide Chart for Operators and Designers

Based on the present analytical models for lower and upper bounds, a computer program entitled as "KAIST-CIWH" has been developed. Using this computer code, a series of $(W_{f,in})_{crit}$ versus L/D curves are obtained for various combinations of flow parameters. The key input parameters for the "KAIST-CIWH" computer code are ① the pipe diameter, ② the system pressure, and ③ the inlet feedwater temperature as shown in Fig. 9(a). Figure 9(b), on the other hand, shows a sample output obtained from the "KAIST-CIWH". This figure shows two sample curves that can be used to find CIWH free regions for given conditions. That is, regions I and III are located outside the upper and lower bounds of the CIWH region, respectively. Therefore, no CIWH is predicted to occur in these regions. The region II, on the other hand, is surrounded by both lower and upper bounds and the CIWH is predicted to occur only in this region.

Two sample guide charts obtained from the KAIST-CIWH code are presented in Figs. 10(a,b) using the pipe diameter (D) and the system pressure (P) as major system parameters. Using the KAIST-CIWH code, one can easily produce a similar guide chart for other conditions depending on the problem.

Table 3. Comparisons of Predicted Critical Feedwater Flow rates by KAIST-CIWH Program and by Eqs. (16) and (17)

		Actual accident	KAIST-CIWH ①	Eqs.(16), (17) ②	(①-②)/① (%)
San Onofre Unit	Upper bound	9.45 kg/s (A, C-loop) (No water hammer)	8.240	8.306	-0.801
	Lower bound	1.58 kg/s (B-loop) (Water hammer)	0.380	0.354	6.842
Sample case study by Izenson et al.	Upper bound	8.665 kg/s (Water hammer)	9.700	9.764	-0.660
	Lower bound	-	0.543	0.500	7.919

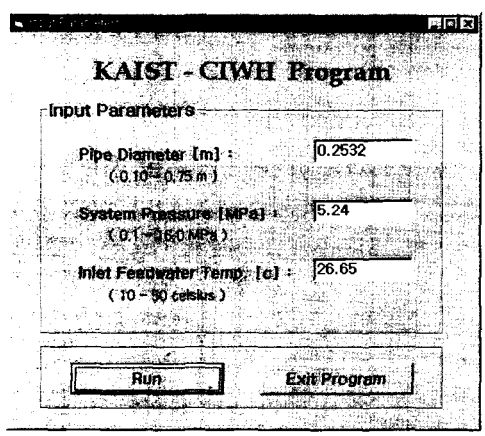

(a) Input form

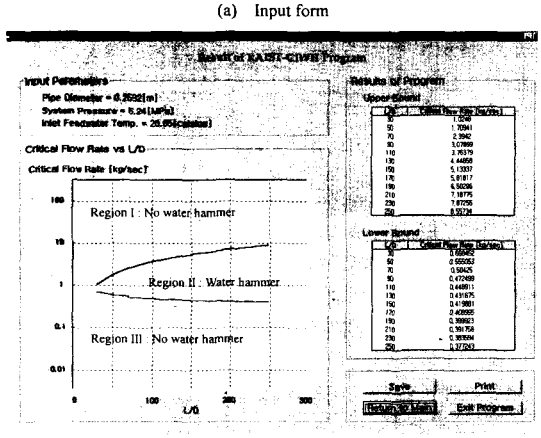

(b) Output form

Fig. 9. KAIST-CIWH Computer Program Printout

4.4. Simple Formulas for Lower and Upper Bounds

The computation time required to produce an output by runing the KAIST-CIWH code depends largely on the pipe diameter (D). For pipe diameters below 0.1 m, it takes less than 20 minutes to get an output from the KAIST-CIWH code, whereas it takes 2~3 hours when pipe diameters are larger than 0.6 m. Therefore, an effort has been made to derive simple formulas for both upper and lower bounds that can be used in an emergency where a quick rather than an accurate result is needed.

Noting that $(W_{f,in})_{crit}$ value for both lower and upper bounds are functions of D, P, $T_{f,in}$, and L/D, a series of sensitivity analysis have been performed with alternating conditional expectation algorithm [15], and the following two simple formulas are obtained:

$$(W^*_{f,in})_{crit,upper} = 0.0032\frac{1-0.9214T^*}{1-0.2720T^*}(D^*)^{-0.5604}\left(\frac{L}{D}\right)^{1.0030} \exp\left[0.3002(P^*)^{0.3245}\right] \quad (16)$$

$$(W^*_{f,in})_{crit,lower} = 1.9352(T^*)^{1.9905}(D^*)^{-0.8433}\left[\frac{1+0.0127\,L/D}{1+0.0450\,L/D}\right] \quad (17)$$

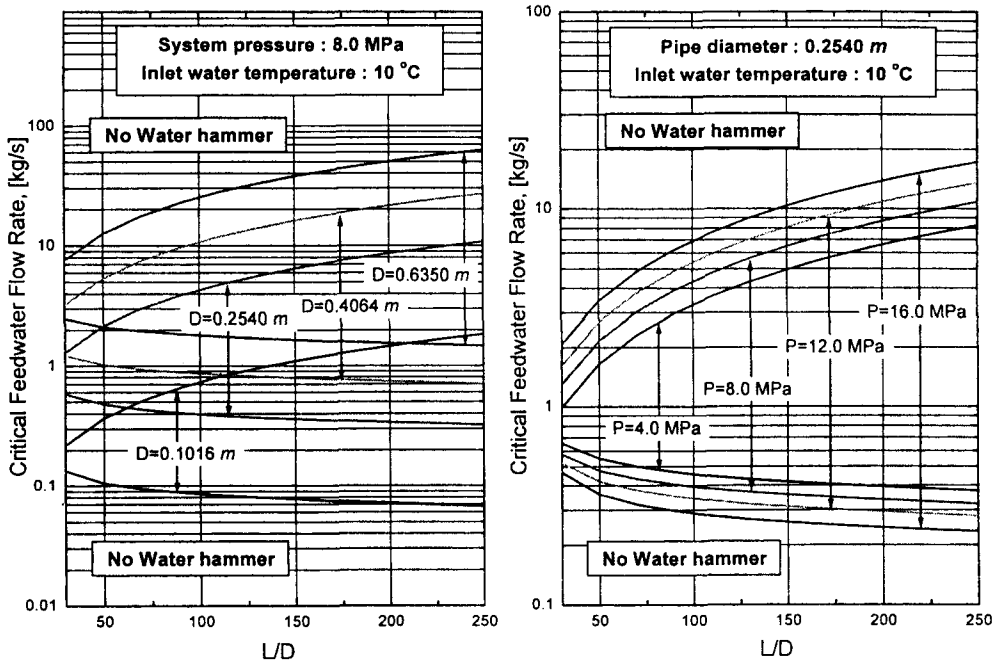

(a) Effect of pipe diameter (b) Effect of system pressure

Fig. 10 Sample Guide Charts to Avoid CIWH Initiation when Pipe Diameter and System Pressure are Used as Major Parameters

where

$(W^*_{f,in})_{crit} = \dfrac{(W_{f,in})_{crit}}{\rho_f A\sqrt{gD}}$ = dimensionless critical feedwater flow rate,

$D^* = D\sqrt{\dfrac{g\rho_f}{\sigma_f}}$ = dimensionless diameter,

$P^* = \dfrac{P_{atm}+P}{P_{atm}}$ = dimensionless system pressure, and

$T^* = \dfrac{T_{f,in}}{T_{sat}}$ = dimensionless inlet feedwater temperature.

It may be noted here that the system pressure (P) does not appear in Eq. (17) for the lower bound. The effect of pressure, however, is included implicitly through T^* which varies according to the system pressure. Also, the ranges of parameters summarized in Table 2 are also applicable for Eqs. (16) and (17).

To examine their applicability and accuracy, Eqs. (16) and (17) have been applied to two CIWHs of San Onofre Unit and Izenson et al.. Predicted $(W_{f,in})_{crit}$ values obtained by Eqs. (16) and (17) are compared with those obtained by KAIST-CIWH program in Table 3. The maximum deviation between the two values is less than 8%. In addition, KAIST-CIWH code has been run 300 times to obtain a total of 3600 data points and they are also compared with the predictions of Eqs. (16) and (17) in Figs. 11(a,b). Both results agree within $\pm 10\%$ for upper bound and $\pm 20\%$ for lower bound, respectively.

5. Summary and Conclusions

The CIWH for steam-water countercurrent flow in a nearly horizontal circular pipe has been studied both experimentally and analytically. The

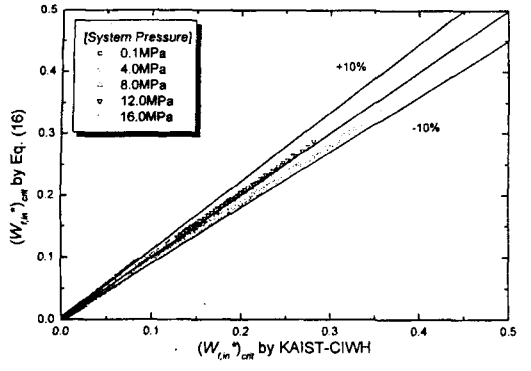

(a) Upper Bound

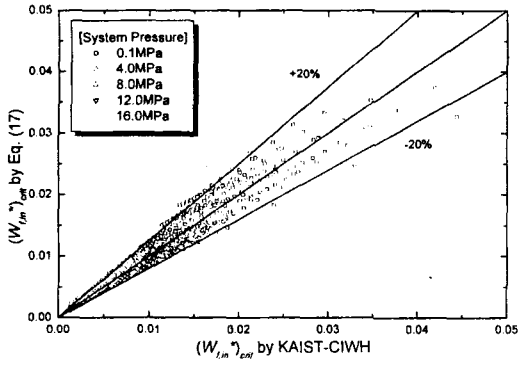

(B) Lower Bound

Fig. 11 Comparison of $(W_{f,in}^*)_{crit}$ Predicted by KAIST-CIWH Program and by Eqs. (16) and (17)

present work may be briefly summarized as follows:

1. A total of 17 experimental data for the onset of slugging have been obtained in a nearly horizontal steam-water countercurrent flow for various flow rates of inlet water.
2. Following existing methods used by earlier workers, incorporating interfacial correlations of h_i and f_i developed particularly for a circular pipe geometry, and using the criterion of transition from stratified to a slug flow developed most recently, two analytical models to obtain $(W_{f,in})_{crit}$ values for both lower and upper bounds of the CIWH initiation have been upgraded.
3. Present models for a CIWH initiation have been tested for their applicability using two sets of CIWH data and also compared with results of existing models. This comparison shows that the present models are reasonably applicable to predict lower and upper bounds of the CIWH initiation.
4. Based on the present analytical models of lower and upper bounds for the CIWH initiation, a computer code entitled as "KAIST-CIWH" has been developed and sample guide charts to find CIWH free regions for a given set of conditions have been presented.
5. To examine the effects of major parameters such as D, P, $T_{f,in}$, and L/D on $(W_{f,in})_{crit}$ of both lower and the upper bounds, a series of $(W_{f,in})_{crit}$ values versus L/D curves are obtained for different combinations of major flow parameters using the "KAIST-CIWH" code, and conclusions are deduced from these curves. In addition, two simple formulas for lower and upper bounds of the CIWH to be used for a quick result in an emergency are also presented.

Acknowledgement

The authors gratefully acknowledge the financial support of the Korea Electric Power Research Institute (KEPRI) through the Center for Advanced Reactor Research (CARR) at the Department of Nuclear Engineering, KAIST.

Nomenclatures

A	area (m^2)
C	constant defined by Eq. (7)
C_p	specific heat ($J\ kg^{-1}\ K^{-1}$)
D	pipe diameter (m)
Fr	Froude number

g	gravitational acceleration (m s^{-2})
h	heat transfer coefficient (W m^{-2} (C^{-1})
δ	depth (m)
i	specific enthalpy (J kg^{-1})
j	superficial velocity (m s^{-1})
L	pipe length (m)
N_{CIWH}	stability parameter in Eq. (6)
P	system pressure (Pa)
Rr	Reynolds number
S	perimeter (m)
T	temperature (K)
V	velocity (m s^{-1})
W	mass flow rate (kg s^{-1})
α	void fraction
θ	inclination angle (radian)
ρ	density (kg m^{-3})
σ	surface tension (N m^{-1})
τ	shear stress (N m^{-2})

Subscript

atm	atmospheric
c	condensation
crit	critical
f	water
g	steam
i	interface
in	inlet
n	node identification
sat	saturation
wa	wall

Superscript

* dimensionless quantity

Appendix A

Definitions of Dimensionless Variables Used in the Dimensionless Governing Equations for Lower Bound of CIWH

Definitions of dimensionless variables in Eqs. (1) ~ (3) are as follows:

$$\delta_f^* = \frac{\delta_f}{D} \qquad x^* = \frac{x}{D} \tag{A1}$$

$$W_f^* = \frac{W_f}{W_{f,in}} \qquad W_g^* = \frac{W_g}{W_{f,in}} \tag{A2}$$

$$\tau_f^* = \frac{\tau_f S_f}{\rho_f g A_f} \qquad \tau_g^* = \frac{\tau_g S_g}{\rho_f g A_g} \qquad \tau_i^* = \frac{\tau_i S_i}{\alpha \rho_f g A_f} \tag{A3}$$

$$T_f^* = \frac{(T_f - T_{f,in})}{(T_g - T_{f,in})} \tag{A4}$$

$$q^* = \frac{\left[h_i S_i (T_g - T_f) + h_{wa} S_g (T_g - T_{wa})\right] A_f}{W_f S_i i_{fg}} \tag{A5}$$

$$\phi = \left(\frac{1-\alpha}{\alpha}\right)\frac{\rho_g V_g^2}{\rho_f V_f^2} \qquad \psi = \left(\frac{1-\alpha}{\alpha}\right)\frac{V_g}{V_f} \tag{A6}$$

$$\beta_0 = \frac{i_g - i_{f,in}}{i_{fg}} \qquad \beta_1 = 1 + \frac{i_g - i_f}{i_{fg}} \qquad \beta_2 = \frac{i_f - i_{f,in}}{i_{fg}} \tag{A7}$$

$$Fr^2 = \frac{V_f^2 S_i}{g A_f} = \frac{W_f^2 S_i}{g \rho_f^2 A_f^3} \tag{A8}$$

Appendix B

Constitutive Relations Used in the Lower and Upper Bounds for CIWH

B.1. Constitutive Relations for Lower Bound

Constitutive relations to obtain τ_i, τ_f, τ_g, h_i, and h_{wa} are as follows: The liquid-wall shear stress τ_f and steam-wall shear stress τ_g are obtained from the basic relation between friction stress τ and friction factor f :

$$\tau = \frac{1}{8} f \rho V^2 \tag{B1}$$

where the friction factor for turbulent flow could be approximated by

$$f = 0.316\,\mathrm{Re}^{-0.25} \tag{B2}$$

In Eq. (B2), Reynolds numbers for liquid and steam are defined as

$$\mathrm{Re}_f = \frac{\rho_f V_f D_{h,f}}{\mu_f}, \qquad \mathrm{Re}_g = \frac{\rho_g V_g D_{h,g}}{\mu_g} \tag{B3 a, b}$$

where $D_{h,f}$ and $D_{h,g}$ are given by

$$D_{h,f} = \frac{4A_f}{S_f}, \qquad D_{h,g} = \frac{4A_g}{S_g + S_i} \tag{B4 a, b}$$

The interfacial shear stress τ_i in a condensing flow is calculated as a linear superposition of the interface shear stress with no condensation and the suction parameter

$$\tau_i = \frac{1}{8} f_{ia} \rho_g V_g^2 + \frac{V_g}{S_i}\frac{dW_f}{dx} \tag{B5}$$

For the nearly horizontal (θ=0.25°) countercurrent air-water flow in circular pipe (D=0.083 m), the empirical correlation for the adiabatic interfacial friction factor was given in KEPRI report [10] as follows.

$$f_{ia} = 1.93\times10^{-14}\,\mathrm{Re}_f^{0.21}\,\mathrm{Re}_g^{2.56} \tag{B6}$$

The local interfacial condensation heat transfer coefficient , on the other hand, is obtained from the correlation of Chu et al. [9] for countercurrent stratified flow of steam and subcooled water at atmospheric pressure in a circular pipe geometry at an inclination of from the horizontal.

$$Nu_i = 4.31\times10^{-3}\,\mathrm{Re}_f^{1.04}\,\mathrm{Re}_g^{0.26}\,\mathrm{Pr}^{0.97} \tag{B7}$$

The local film condensation heat transfer coefficient on the wall can be obtained from the modified Nusselt correlation as follows:

$$h_{wa} = F\left[\frac{\rho_f(\rho_f-\rho_g)g\,k_f^3\,i'_{fg}}{D\mu_f(T_g - T_{wa})}\right]^{1/4} \tag{B8}$$

where

$$F = 0.31\left[\frac{W_g D}{A_g \mu_g}\right]^{0.12} \tag{B9}$$

in the wavy, slug and plug flow regime, and

$$i'_{fg} = i_{fg} + \frac{3}{8} C_{pf}(T_g - T_{wa}) \tag{B10}$$

In the above equation, T_{wa} is approximated by

$$\frac{T_g + T_f}{2}.$$

B.2. Constitutive Relations for Upper Bound

The approximate average heat transfer coefficients *hi* and *hwa* are obtained from the result of Brucker and Sparrow [16] and the modified Nusselt correlation, respectively. The approximate value of the average steam-water interface condensation coefficient is

$$h_i \cong 10^4\ (W/m^2\ ^\circ C) \tag{B11}$$

whereas that for the pipe wall is

$$h_{wa} = 0.56\left[\frac{\rho_f(\rho_f-\rho_g)g\,k_f^3\,i'_{fg}}{D\mu_f(T_g - T_{wa})}\right]^{1/4} \tag{B12}$$

Reference

1. Yow, W., Van Duyne, D.A., Chiu, Chong, 1988. Analysis of root causes of water hammer. 3rd Int. Topical Meeting on Nuclear Power Plant Thermal Hydraulics and Operations (NUPTHO-3), A10-103~109.
2. D. A. Van Duyne, W. Yow, and J. W. Sabin, Water Hammer Prevention, Mitigation, and Accommodation. EPRI NP-6766 (1992).
3. J. A. Block, P. H. Rothe, C. J. Crowley, and G. B. Wallis, An Evaluation of PWR Steam

Generator Water Hammer, NUREG-0291 (1977).
4. M. G. Izenson, P. H. Rothe, and G. B. Wallis, Diagnosis of Condensation-Induced Water hammer, NUREG/CR-5220 (1988).
5. R. W. Bjorge and P. Griffith, "Initiation of water hammer in horizontal and nearly horizontal pipes containing steam and subcooled water," ASME J. Heat Transfer, 106, 835-840 (1984).
6. J. H. Linehan, M. Petrick, and M. M. El-Wakil, "The condensation of a saturated vapor on a subcooled film during stratified flow," AIChE Progress Symposium Series, 66, 11-20 (1970).
7. Y. Taitel and A. E. Dukler, "A model for predicting flow regime transitions in horizontal and near horizontal gas-liquid flow," AIChE J., 22, 47-55 (1976).
8. M. H. Chun and C. K. Sung, "Onset of slugging criterion based on characteristics and stability analyses of transient one-dimensional two-phase flow equations of two-fluid model," Int. Comm. Heat Mass Transfer, 23, 473-484 (1996).
9. I. C. Chu, S. O. Yu, and M. H. Chun, "Interfacial condensation heat transfer for countercurrent steam-water stratified flow in a horizontal circular pipe," First Korea-Japan Symposium on Nuclear Thermal Hydraulic and Safety (NTHAS98), 299-306 (1998).
10. Chun et al., Development of a Model for Analysis of the Water Hammer in NPP and the Evaluation of Thermo-Hydraulic Design of RCS, Korea Electric Power Research Institute, TR.95ZJ16.J1999.115 (1999).
11. M. H. Chun and H. Y. Nam, "Analysis of water hammer induced by steam-water counterflow in a long horizontal pipe," Int. Comm. Heat Mass Transfer, 19, 507-518 (1992).
12. C. Chiu, D. Tuttle, and A. W. Serkiz, "Water hammer in a PWR horizontal feedwater line," ANS Trans., 52, 589-590 (1986).
13. Y. Chou and P. Griffith, "Admitting cold water into steam filled pipes without water hammer due to steam bubble collapse," Nuclear Engineering and Design, 121, 367-378 (1990).
14. A. B. Jackobek and P. Griffith, Investigation of Cold Leg Water Hammer in a PWR Due to the Admission of Emergency Core Cooling During a Small Break LOCA, NUREG/CR-3895 (1984).
15. L. Breiman and J. H. Friedman, "Estimating optimal transformations for multiple regresseion and correlation," J. Am. Stat. Assoc., 80, 580-598 (1985).
16. G. G. Brucker and E. M. Sparrow, "Direct contact condensation of steam bubbles in water at high pressure," Int. J. Heat Mass Transfer, 20, 371-381 (1977).